Non-Isothermal Three-Dimensional Developments and Process Modeling of Composites: Flow/Thermal/Cure Formulations and Experimental Validations

N. D. Ngo, K. K. Tamma[1]

Abstract: In the process modeling via Resin Transfer Molding (RTM) for thick composite sections, multi-layer preforms with varying thermophysical characteristics across the different layers, or for geometrically complex mold geometries with varying thicknesses, the assumption of a thin shell-like geometry is no longer valid. The flow in the through thickness direction is no longer negligible and current practices of treating the continuously moving flow front as two-dimensional and the temperature and cure as three-dimensional are not representative of the underlying physics. In view of these considerations, in the present study, the focus is on the non-isothermal process modeling of composites employing full three-dimensional modeling/analysis developments via effective computational techniques. The specific applications are for thick composite geometries where the thickness is comparable to the other dimensions of the part. For the first time, an implicit pure finite element front tracking technique is employed for the transient flow/thermal/cure coupled behavior of the full three-dimensional modeling of the moving boundary value problem, and, due to the highly advective nature of the non-isothermal conditions involving thermal and polymerization reactions, special considerations and stabilization techniques are proposed. Validations and comparisons with available experimental results are particularly emphasized and demonstrated.

keyword: resin transfer molding, non-isothermal simulation, finite element method, process modeling of composites

1 Introduction

In today's industries, advanced composites made of fiber-reinforced polymer resin are increasingly being used due to their excellent weight-to-performance ratios, cheap toolings, short mold manufacturing and tryout times, design flexibility, noncorrosive nature, and ability to manufacture consolidated parts of complex geometric shapes. Presently, among the various polymeric matrix composite manufacturing techniques employed in industry, the process of resin transfer molding (RTM) is being recognized as one of the more attractive manufacturing processes due to its high performance in structural integrity issues and low energy consumption requirements.

[1] Department of Mechanical Engineering, Institute of Technology, 111 Church Street S.E., University of Minnesota, Minneapolis, MN 55455, USA. Phone : 612-625-1821 Fax : 612-624-1398

Technically, the RTM manufacturing process involves the injection of resin into a mold cavity filled with porous fiber mat. A dry porous fiber preform is first cut into specific shapes, stacked and placed inside a mold cavity in desired orientations. The mold is then closed and a reactive polymer resin initially at a low viscosity is injected under pressure through one or more injection ports. During this process, the liquid resin flows through the fiber preform, impregnating or wetting the fiber tows. After the resin has completely impregnated the fiber preform in the mold cavity, the mold is heated and the part is cured with the liquid resin undergoing polymerization reactions to become a structural solid. Once curing completes, the consolidated net-shape part is removed from the mold. The overall success of the RTM manufacturing process thus depends on the complete impregnation of the fiber mat by the polymer resin, prevention of polymer gellation during filling, and subsequent avoidance of dry spots. Since a cold resin is injected into a hot mold, the associated physics encompasses a moving boundary value problem in conjunction with the multi-disciplinary study of flow/thermal and cure kinetics inside the mold cavity. Although experimental validations are indispensable, routine manufacture of large complex structural geometries can only be enhanced via computational simulations, thus eliminating costly trial runs and helping designers in the set-up of the manufacturing process.

In general, the study of the RTM process modeling in literature can be divided into two categories: isothermal and non-isothermal RTM processes. The study of isothermal RTM process modeling centers around the use of Darcy's law to describe the flow of resin through the fiber preforms and the tracking of the flow fronts as the resin enters the cavity during filling. Research issues pertinent to the process modeling area include: characterization of fiber mat permeabilities, conductivity, structural constitution, kinetics models, and computational efforts to enhance and/or shed light on the various mechanism and physics associated with RTM. While various computational techniques have been used to accomplish the task of flow front tracking, over the years, the two most popular techniques have been:

1. Lagrangian front tracking technique where a numerical mesh continuously enlarges and deforms in conformity over the fluid domain as the fluid fills the mold cavity;

2. Eulerian front tracking technique where a fixed mesh is

formed over entire mold cavity and the fluid is allowed to impregnate the fixed mesh.

In the Lagrangian technique, new meshes have to be continuously generated at every time step and considerable effort is needed in this approach to generate acceptable meshes. While this method can provide accurate representation of the front surface and the interface, it becomes quite cumbersome when complex geometries and diverging/merging flow fronts are involved. An example of this moving mesh technique is the boundary-fitted coordinate system. In the Eulerian technique, only one mesh is required to be generated at the beginning of the analysis to define the mold geometry. This single-mesh-generation approach reduces the amount of computer usage considerably but has the disadvantage of not giving the exact location of the flow front at any instant in time. The reason behind this technical difficulty is that in the fixed mesh technique, the flow front is typically located by interpolating a nodal parameter among the nodes of the fixed mesh. As a consequence, the accuracy of the flow front calculation suffers with the coarseness of the mesh and the employed interpolation scheme. Currently, the so-called Control Volume/Finite Element (CV-FE) explicit formulation is one of the more traditional methods used to track the flow front in the fixed mesh category; although more recent efforts by Ngo, Mohan, Chung, and Tamma (1997); Mohan, Shires, Tamma, and Ngo (1998); Mohan, Ngo, and Tamma (1999a,b); Mohan, Ngo, Tamma, and Shires (1999) have shown significant enhancements via a viable alternative formulation termed the Pure FE implicit methodology which accurately accounts for the transient nature of the problem, ensures mass conservation, and avoids the notion of having to associate control volumes in a finite element mesh and computation of flow rates.

In the study of non-isothermal RTM process, the additional focus is on the heat transfer equation and the curing kinetics, as well as the viscosity models, of the resin. Current review of published literature [Bruschke and Advani (1994); Liu and Advani (1995); Chan and Hwang (1992, 1993); Lin, Lee, and Liou (1991); Lee, Young, and Lin (1994); Young (1994, 1995); Trochu, Gauvin, and Zhang (1992); Trochu, Gauvin, and Gao (1993); Trochu, Boudreault, Gao, and Gauvin (1995); Gao, Trochu, and Gauvin (1995)] indicates that in the RTM process, the heat transport equation can in general be based on either a two-phase model or a local equilibrium model. The two-phase model involves the separate calculations of the resin and the fiber energy balance, with the heat exchange between the resin and the fiber preform being taken into account via the introduction of an interfacial heat exchange. In most cases, the heat transfer coefficient required in the definition of the interfacial heat exchange cannot be determined theoretically; experimental procedures must be used to determine the coefficient h for each fiber/resin combination based on the assumption that the heat transfer coefficient h is flow rate dependent. If the RTM process can be assumed to be in local thermal equilibrium (i.e., the temperature is the same at a local position for both the resin fluid and the fiber preform), then the separate energy balance equations can be combined into one equation and the effective material properties can be determined using appropriate averaging techniques. This assumption is adequate when the heat transfer coefficient between the fiber and the resin is large, or when the resin flow is very slow [Lee, Young, and Lin (1994)]. At the present time, there is no universal agreement on what models to use for the chemorheology and curing of the resins. Most models are empirical and different resins may be best described by different models.

Although not often covered in the modeling of the RTM processes by most researchers, thermal dispersion is a phenomenon that might be considered when applying porous media theory to the area of fiber-reinforced composites manufacturing by liquid composite molding processes. Dessenberger and Tucker (1995) described from their study that under certain conditions, thermal dispersion can be important in RTM mold filling. They explained that physically, dispersion occurs because the microscopic fluid velocities and temperatures are different from the average values, and demonstrated that numerical predictions based on a local volume-averaged energy equation only agreed well with experimental data when thermal dispersion was included in the model. They also showed that it was possible to match temperatures at different locations under various operating conditions with a single dispersion model. However, Dessenberger and Tucker (1995) noted that the dispersion model developed in their study had some difficulty matching the experimental temperatures in the lower Peclet number regimes and that further studies would be necessary to work out the details of dispersion modeling in these regimes.

In the present study, new computational developments are described for the first time which effectively account for the representative physics and thereby permit an accurate three-dimensional modeling/analysis approach for process modeling of composites manufactured by RTM. The emphasis is on the non-isothermal process modeling of RTM composites employing full three-dimensional modeling/analysis computational developments in conjunction with a viable moving front technique. This is the first time such computations have been performed with the implicit Pure FE front tracking technique for three-dimensional flow/thermal/cure simulations. Validations with available experimental results are subsequently performed to demonstrate the overall effectiveness of the proposed efforts. The overall computational developments are excerpts of a general-purpose in-house research code titled "OCTOPUS" (On Composites Technology Of Polymeric Useful Structures) which inherits a vast finite element library, filling techniques, time integrators, stabilizing features and constitutive models for applications to practical large scale composite geometries. In the next section, the theory of local volume averaging and the volume-averaged balance equations for mass,

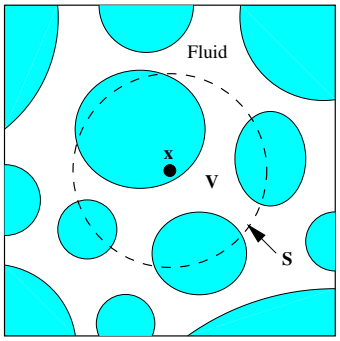

Figure 1 : Schematic of an averaging volume V and its surface S.

momentum, energy and chemical reaction are first discussed, albeit briefly, to allow for a better understanding of the constitutive modeling equations. Theoretical developments are then described and followed by simulations and validations.

2 Volume-Averaged Equations

Due to the differences in the length scales that exist in the RTM process, namely, (i) the region within the woven fiber preform at the length scale of the tow diameters and (ii) the region within the yarns at the length scale of the individual fibril diameters, it is often not practical, if not impossible, to model the intricate geometric details of the RTM process such as flow, temperature and cure at the *microscopic* level. Therefore, when dealing with a porous medium, a common practice is to introduce the idea of *local volume averaging* and the use of average quantities in the field equations [Kaviany (1995); Tucker and Dessenberger (1994)].

In the RTM process, the domain typically contains two phases: the resin and the woven fiber mat. These two phases are termed *fluid* and *solid*, respectively, and are denoted by the subscripts "f" and "s". Fig. 1 shows the representative volume V and the associated enclosing surface S of an arbitrary point $\mathbf{x}$. Since detailed derivations of the volume-averaged mass, momentum, energy and chemical reaction equations are clearly beyond the scope of the present paper, the current developments will only highlight the mass, momentum, energy and chemical reaction equations in their final volume-averaged forms. Interested readers are referred to the work of Kaviany (1995); Tucker and Dessenberger (1994) for further details.

2.1 Local Volume Averaging of Continuity Equation

For an incompressible fluid, following the standard procedures, the volume-averaged continuity equation is given as

$$\nabla \cdot \langle \mathbf{u}_f \rangle = 0 \tag{1}$$

2.2 Local Volume Averaging of Momentum Equation

With the assumption of incompressibility, the volume average of the momentum equation is derived as

$$\rho_f \frac{\partial \langle \mathbf{u}_f \rangle}{\partial t} + \rho_f \langle \mathbf{u}_f \cdot \nabla \mathbf{u}_f \rangle = -\nabla \langle P_f \rangle + \mu \nabla \cdot \nabla \langle \mathbf{u}_f \rangle - \frac{\mu}{K} \langle \mathbf{u}_f \rangle \tag{2}$$

where ρ_f is the fluid density, μ is the fluid viscosity and K is the permeability of the porous medium and P_f is the *modified pressure* defined as

$$P_f = p_f + \rho_f g h \tag{3}$$

2.2.1 The Brinkman Equation

With regards to the volume-averaged momentum equation, Equation (2), if the fluid is assumed Newtonian with a constant viscosity and if the inertia term is negligible as can be done for porous media flow, then one arrives at

$$-\nabla \langle P_f \rangle + \mu \nabla \cdot \nabla \langle \mathbf{u}_f \rangle - \frac{\mu}{K} \langle \mathbf{u}_f \rangle = 0 \tag{4}$$

which is similar to the momentum balance first proposed and used by Brinkman (1947).

2.2.2 Darcy's Law

In addition, in many porous media flow problems, the length scale over which the average velocity $\langle \mathbf{u}_f \rangle$ changes is much larger than the local pore scale [Tucker and Dessenberger (1994)]. When such is the case, an order-of-magnitude analysis reveals that the divergence of the volume-averaged viscous stress is much smaller than the Darcy resistance term. Hence, the momentum balance equation Equation (4) reduces to

$$-\nabla \langle P_f \rangle - \frac{\mu}{K} \langle \mathbf{u}_f \rangle = 0 \tag{5}$$

or

$$\langle \mathbf{u}_f \rangle = -\frac{1}{\mu} K \nabla \langle P_f \rangle \tag{6}$$

which is the classical Darcy's law [Darcy (1856)]. To account for the anisotropy of the material properties encountered in porous media flows in general, and in the RTM process in particular, the isotropic K in Darcy's law is often replaced by a tensorial $\overline{\mathbf{K}}$ to give

$$\langle \mathbf{u}_f \rangle = -\frac{1}{\mu} \overline{\mathbf{K}} \cdot \nabla \langle P_f \rangle \tag{7}$$

2.3 Local Volume Averaging of Energy Equation

In dealing with the heat transport phenomenon in the RTM process, two options exist for setting up the energy equation:

either (i) a *two-phase* model where the fluid and solid temperatures are treated separately, or (ii) the *local thermal equilibrium* model where the fluid and solid temperatures are assumed to be the same at a local position. While both models have been used to model the RTM process [Bruschke and Advani (1994); Liu and Advani (1995); Chan and Hwang (1992, 1993); Lin, Lee, and Liou (1991); Lee, Young, and Lin (1994); Young (1994, 1995); Trochu, Gauvin, and Zhang (1992); Trochu, Gauvin, and Gao (1993); Trochu, Boudreault, Gao, and Gauvin (1995); Gao, Trochu, and Gauvin (1995)], the local thermal equilibrium model is generally preferred over the two-phase model due to its simplicity and is less intensive computationally.

The volume-averaged energy equation for the thermal equilibrium model is

$$\left(\phi_f \rho_f c_{pf} + \phi_s \rho_s c_{ps}\right) \frac{\partial \langle T \rangle}{\partial t} + \rho_f c_{pf} \langle \mathbf{u}_f \rangle \cdot \nabla \langle T \rangle = \nabla \cdot (\mathbf{k}_e + \mathbf{k}_D) \cdot \nabla \langle T \rangle + \phi_f \langle \dot{G}_f \rangle^f \tag{8}$$

where ρ_f and ρ_s are the fluid and solid density, c_{pf} and c_{ps} are the fluid and solid specific heat, ϕ_f is the porosity of the porous medium, T is the local thermal equilibrium temperature and $\dot{G}_f$ is the rate of energy dissipation per unit volume in the fluid phase. Superscript "f" is used here to denote the fluid *intrinsic phase average* of the variable and ϕ_s is the solid volume fraction of the porous medium defined by

$$\phi_s = 1 - \phi_f \tag{9}$$

In Equation (8), $\mathbf{k}_e$ is the effective conductivity tensor defined as

$$\mathbf{k}_e = (\phi_f k_f + \phi_s k_s)\,\mathbf{I} + \frac{k_f - k_s}{V} \int_{S_{fs}} \mathbf{n}_{fs} \mathbf{b}\, dS \tag{10}$$

where k_f and k_s are the fluid and solid thermal conductivity, $\mathbf{I}$ is the identity matrix, S_{fs} is the fluid-solid interface, and $\mathbf{b}$ is the vector function that transforms the gradient of the average temperature into the local variation of the deviation from the average temperature [Tucker and Dessenberger (1994)]. $\mathbf{k}_D$ in Equation (8) is the thermal dispersion conductivity tensor whose values are determined through either experimental means or computational measures if an explicit unit cell could be readily identified. Specifically, from the local volume averaging techniques, the thermal dispersion conductivity tensor is derived to be

$$\mathbf{k}_D = -\phi_f \rho_f c_{pf} \langle \hat{\mathbf{u}}_f \mathbf{b} \rangle^f \tag{11}$$

where $\hat{\mathbf{u}}_f$ is the deviation of the local velocity from the average value and is given by

$$\mathbf{u}_f = \langle \mathbf{u}_f \rangle + \hat{\mathbf{u}}_f \tag{12}$$

If a unit cell could be defined, then in principle the Navier-Stokes equation could be used to solve for the velocity field in the entire cell using periodic boundary conditions and the pointwise velocity deviation, $\hat{\mathbf{u}}_f$, could in theory be calculated.

2.4 Local Volume Averaging of Species Mass Balance Equation

For the curing reaction of the resin, the volume average of the governing species mass balance equation takes the form:

$$\phi_f \frac{\partial \langle \alpha_f \rangle^f}{\partial t} + \langle \mathbf{u}_f \rangle \cdot \nabla \langle \alpha_f \rangle^f = \phi_f \nabla \cdot \mathbf{D}_D \cdot \nabla \langle \alpha_f \rangle^f + \phi_f \langle R_f \rangle^f \tag{13}$$

where $\mathbf{D}_D$ is the thermal dispersion tensor given by

$$\mathbf{D}_D = -\frac{1}{V_f} \int_{V_f} \hat{\mathbf{u}}_f \mathbf{b}\, dV = \langle \hat{\mathbf{u}}_f \mathbf{b} \rangle^f \tag{14}$$

and R_α is the rate of chemical reaction. In the remainder of this paper, the volume-averaged constitutive equations are written without the $\langle\ \rangle$ brackets and ϕ is used in place of the porous medium porosity ϕ_f.

3 Non-Isothermal 3-D Formulations

For thick composite sections, multi-layer preforms with varying characteristics across the different layers, the assumption of a thin shell-like geometry is no longer valid. The flow in the through thickness direction is no longer negligible and the 2-D flow/3-D thermal formulations [Ngo and Tamma (1999, 2000)] are not representative of the underlying physics. To address these shortcomings, formulations with full three-dimensional physics must be developed to model and account for the three-dimensional nature of the flow field, as well as those of the thermal and curing fields. In the present developments, the focus is on the theoretical developments and validations of the non-isothermal three-dimensional pure finite-element based methodology. As such, emphasis is placed on: (i) the theoretical developments, (ii) the computational methodology for flow/thermal/cure coupling, and (iii) the validations of the formulations with available experiments. The finite element developments for pressure, temperature and cure are first described. These are then followed a detailed computational methodology for coupling the flow/thermal/cure transient moving boundary value problem.

3.1 Pressure Solution

In the process modeling of thick composite sections undergoing the RTM process the flow is three-dimensional. The governing equation for the fill factor Ψ and pressure P in the present Pure FE methodology [Ngo, Mohan, Chung, and Tamma (1997); Mohan, Shires, Tamma, and Ngo (1998); Mohan, Ngo, and Tamma (1999a,b); Mohan, Ngo, Tamma, and Shires (1999)] is

$$\frac{\partial \Psi}{\partial t} = \nabla \cdot \left(\frac{\overline{\mathbf{K}}}{\mu} \nabla P \right) \tag{15}$$

with the following boundary and initial conditions:

At mold surface:	$\frac{\partial P}{\partial n} = 0$ on Γ_1
At resin front:	$P = 0$ on Γ_2
At mold inlet:	$P = P_0$ (prescribed pressure)
	or $q = q_0$ (prescribed flow rate),
	and $\Psi = 1$
Initially:	$\Psi(t=0) = 0$

Invoking the traditional weighted residual formulation yields

$$\int_\Omega \mathbf{W}^T \frac{\partial \Psi}{\partial t} d\Omega = \int_\Omega \mathbf{W}^T \left(\nabla \cdot \frac{\overline{\mathbf{K}}}{\mu} \nabla P \right) d\Omega \tag{16}$$

where $\mathbf{W}$ are the weighting functions. If $\mathbf{W}$ are taken to be the same as shape functions $\mathbf{N}$ and approximating

$$\begin{aligned} \Psi &= N_i \Psi_i \\ P &= N_i P_i \end{aligned} \tag{17}$$

Equation (16) becomes

$$\left[\int_\Omega N_i N_j d\Omega \right] \frac{\partial \Psi_j}{\partial t} = \left[- \int_\Omega \nabla N_i \frac{\overline{\mathbf{K}}}{\mu} \nabla N_j d\Omega \right] P_j + \int_\Gamma N_i \left(\frac{\overline{\mathbf{K}}}{\mu} \nabla P \right) \cdot \mathbf{n} d\Gamma \tag{18}$$

For an incompressible porous medium, a three-dimensional version of Darcy's law can be used to describe the pressure/flow rate relationship in a medium with anisotropic permeability as

$$\begin{Bmatrix} \overline{u}_x \\ \overline{u}_y \\ \overline{u}_z \end{Bmatrix} = -\frac{1}{\mu} \begin{bmatrix} \overline{K}_{xx} & \overline{K}_{xy} & \overline{K}_{xz} \\ \overline{K}_{yx} & \overline{K}_{yy} & \overline{K}_{yz} \\ \overline{K}_{zx} & \overline{K}_{zy} & \overline{K}_{zz} \end{bmatrix} \begin{Bmatrix} \frac{\partial P}{\partial x} \\ \frac{\partial P}{\partial y} \\ \frac{\partial P}{\partial z} \end{Bmatrix} \tag{19}$$

3.2 Temperature Solution

In addition to the three-dimensional nature of the flow field, the heat transfer must also be treated in three dimensions because the heat convection in the planar direction and the heat conduction in the gapwise direction are both important. The heat transfer equation based on the thermal equilibrium model is given by

$$\rho c_p \frac{\partial T}{\partial t} + \rho_f c_{pf} (\mathbf{u} \cdot \nabla T) = \nabla \cdot \mathbf{k} \nabla T + \phi \dot{G} \tag{20}$$

where ϕ is the porosity of the porous medium and subscripts "f" and "s" denote the fluid or resin and the solid or fiber, respectively. The material properties ρ and c_p are the average density and specific heat whose values are weighted according to:

$$\rho c_p = \phi \rho_f c_{pf} + (1-\phi) \rho_s c_{ps} \tag{21}$$

and $\mathbf{k}$ is the effective thermal conductivity defined as

$$\mathbf{k} = \mathbf{k}_e + \mathbf{k}_D \tag{22}$$

where $\mathbf{k}_e$ is the effective stagnant thermal conductivity given by

$$\mathbf{k}_e = [\phi k_r + (1-\phi) k_f] \mathbf{I} \tag{23}$$

and $\mathbf{k}_D$ is the thermal dispersion conductivity. The initial and boundary conditions for the thermal equilibrium energy equation are:

At mold wall:	$T = T_w$
At mold inlet:	$T = T_{f0}$ during filling
At resin front:	$k \frac{\partial T}{\partial n} = (1-\phi) \rho_f c_{pf} \, \mathbf{u} \cdot \mathbf{n} (T_{s0} - T)$
Initially:	$T(t=0) = T_w$

Invoking the traditional weighted residual formulation and approximating the temperature field T by

$$T = N_i T_i \tag{24}$$

where $\mathbf{N}$ are the finite-element shape functions, Eq.(20) becomes

$$\begin{aligned} &\left(\int_\Omega W_i \rho c_p N_j d\Omega \right) \frac{\partial T_j}{\partial t} \\ &\quad + \left(\int_\Omega W_i \rho_f c_{pf} \mathbf{u} \cdot \nabla N_j d\Omega \right) T_j \\ &\quad + \left(\int_\Omega \nabla W_i \mathbf{k} \nabla N_j d\Omega \right) T_j \\ &\quad = \int_\Gamma W_i (-\mathbf{q} \cdot \mathbf{n}) \, d\Gamma + \int_\Omega W_i \phi \dot{G} d\Omega \end{aligned} \tag{25}$$

where the first term on the right hand side of Equation (25) is obtained using integration by parts. In Equation (25), W_i are the Streamline Upwind Petrov-Galerkin (SUPG) weighting functions employed in the present non-isothermal 3-D formulations for stability considerations of the temperature field. These Petrov Galerkin weighting functions are defined as [Brooks and Hughes (1982)]

$$W_i = N_i + \lambda (\mathbf{u} \cdot \nabla N_i) \tag{26}$$

where λ is a scalar coefficient.

3.3 Cure Solution

With the assumption of negligible thermal dispersion $\mathbf{D}_D$, the three-dimensional species mass balance equation is

$$\phi \frac{\partial \alpha}{\partial t} + \mathbf{u} \cdot \nabla \alpha = \phi R_\alpha \tag{27}$$

with the following boundary and initial conditions:

At mold inlet $\alpha = 0$ during filling
Initially: $\alpha(t=0) = 0$

Invoking the traditional weighted residual method and using finite element approximations

$$\alpha = N_i \alpha_i \tag{28}$$

the discretized system of equations for the cure solution is

$$\left[\int_\Omega W_i \phi N_j d\Omega\right] \frac{\partial \alpha_j}{\partial t} + \left(\int_\Omega W_i \mathbf{u} \cdot \nabla N_j d\Omega\right) \alpha_j = \int_\Omega W_i \phi R_\alpha d\Omega \tag{29}$$

where W_i are the SUPG weighting functions defined by [Brooks and Hughes (1982)]

$$W_i = N_i + \lambda (\mathbf{u} \cdot \nabla N_i) \tag{30}$$

and N_i are the standard finite element shape functions.

4 Flow/Thermal/Cure Integrated Methodology

In the modeling of the non-isothermal RTM process, the 3-D methodology is plagued by the complex coupling of the pressure, temperature and cure solutions. The flow depends on the heat transfer and the chemical reaction through the viscosity of the resin, and the heat transfer and the chemical reaction, in turn, depend on the flow through the convection of the fluid. The total integration of the flow/thermal/cure equations is therefore deemed very important in order to accurately model the physics of the RTM process.

At the beginning of the simulation, the fill factors are taken to be unity at the injection ports and are thus defined. The viscosity field is assumed known from the initial temperatures and degrees of cure. Starting with the very first fill time step, the calculations of the three-dimensional pressure, temperature and conversion fields are given as follows:

1. At the beginning of each fill time step, assume a viscosity field based on the three-dimensional temperature and conversion solutions of the previous time step:

   $$\mu = \mu (\mathbf{T}_n, \boldsymbol{\alpha}_n) \tag{31}$$

   where subscript n denotes the previous time increment.

2. Iterate for the pressure P and the fill factor Ψ using procedures for the Pure FE methodology following Ngo, Mohan, Chung, and Tamma (1997); Mohan, Shires, Tamma, and Ngo (1998); Mohan, Ngo, and Tamma (1999a,b); Mohan, Ngo, Tamma, and Shires (1999).

3. Using the converged pressure field, solve for the velocity field according Darcy's law,

   $$\mathbf{u} = -\frac{\overline{\mathbf{K}}}{\mu} \nabla P \tag{32}$$

   where $\overline{\mathbf{K}}$ is the second-order permeability tensor.

4. Begin sub-time stepping of the fill time increment to solve for the three-dimensional temperature and conversion fields:

   a. Initialize temperature and degree of cure by setting

      $$\mathbf{T}_m = \mathbf{T}_n \quad \text{and} \quad \boldsymbol{\alpha}_m = \boldsymbol{\alpha}_n \tag{33}$$

      where subscript n denotes the previous *fill* time step and subscript m refers to the previous *thermal* time step.

   b. Compute the required number of sub-time steps based on the Courant criterion of unity and the condition set forth by

      $$N\text{steps} = \text{nint}\left(\frac{\Delta t_{filling}}{\Delta t_{equivalent}}\right) \tag{34}$$

      where $\Delta t_{equivalent}$ is the smallest of all the thermal time increments computed at the element level, and "nint" is the nearest integer operation. The thermal time step is given by

      $$\Delta t_{thermal} = \frac{\Delta t_{filling}}{N\text{steps}} \tag{35}$$

   c. Compute the rate of reaction R_α using the appropriate kinetics model (e.g., step-wise or two-step kinetics model) and the temperature and the degree of cure evaluated at the previous thermal time step; thus,

      $$R_\alpha = R_\alpha (\mathbf{T}_m, \boldsymbol{\alpha}_m) \tag{36}$$

      The heat generated due to curing is proportional to the rate of reaction and is given by

      $$\dot{G} = H_R R_\alpha \tag{37}$$

      where H_R is the heat of reaction per unit volume for pure resin.

   d. Form the various mass and stiffness matrices, as well as load vectors, required in the discretized systems of equations for the temperature solution using Equation (25).

   e. Using the trapezoidal θ-family of integration schemes, rearrange the above discretized system of equations into known (i.e., $\mathbf{T}_m$) and unknown (i.e., $\mathbf{T}_{m+1}$) values of temperature. Note that the subscript m refers to the previous thermal time step, while $(m+1)$ denotes the current thermal time step. The modified system of equations to solve for $\mathbf{T}_{m+1}$ is

      $$\hat{\mathbf{K}}_{m+1} \mathbf{T}_{m+1} = \hat{\mathbf{K}}_m \mathbf{T}_m + \hat{\mathbf{F}}_{m,m+1} \tag{38}$$

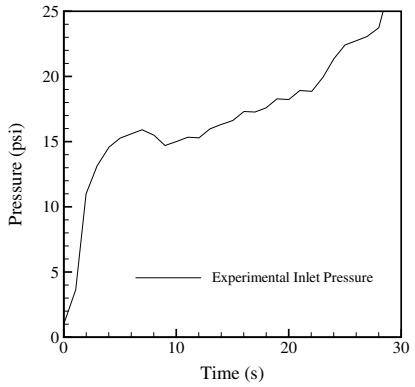

Figure 2 : Recorded inlet pressure of Experiment #1 during filling Lin, Lee, and Liou (1993).

Table 1 : Material properties: Experiment #1

Parameter	Value
Polyurethane Resin	
Density ρ_f (g/cm^3)	1.14
Heat capacity c_{pf} (J/g·K)	1.6747
Thermal conductivity k_f (J/cm·s·K)	0.0015
Heat of reaction H_r (J/g)	108.1
Fiber	
Density ρ_s (g/cm^3)	2.56
Heat capacity c_{ps} (J/g·K)	0.67
Thermal conductivity k_s (J/cm·s·K)	0.0067
Porosity ϕ	0.81
Permeability $\overline{K}$ (cm^2)	3.4E−5

f. Apply prescribed boundary conditions to Equation (38):
   - Prescribed inlet temperature: $T = T_{f0}$ at injection port.
   - Prescribed wall temperature: $T = T_w$ at mold interface.

g. Solve for $\mathbf{T}_{m+1}$.

h. Form the various mass and stiffness matrices, as well as load vectors, required in the discretized systems of equations for the degree of cure using Equation (29).

i. Rearrange the discretized systems of equations into known (i.e., $\boldsymbol{\alpha}_m$) and unknown (i.e., $\boldsymbol{\alpha}_{m+1}$) values of the degree of cure. The modified system of equations to solve for $\boldsymbol{\alpha}_{m+1}$ is

$$\hat{\mathbf{K}}_{m+1}\boldsymbol{\alpha}_{m+1} = \hat{\mathbf{K}}_m\boldsymbol{\alpha}_m + \hat{\mathbf{F}}_{m,m+1} \tag{39}$$

j. Apply prescribed boundary conditions to Equation (39):
   - Prescribed inlet conversion: $\alpha = 0$ at injection port.

k. Solve for $\boldsymbol{\alpha}_{m+1}$.

l. Check for subscript $(m+1)$ being equal to the number of sub-time steps. It $(m+1)$ is not equal to Nsteps, set

$$\mathbf{T}_m = \mathbf{T}_{m+1} \quad \text{and} \quad \boldsymbol{\alpha}_m = \boldsymbol{\alpha}_{m+1} \tag{40}$$

and proceed to the next sub-time step by looping back to Step c. If $(m+1)$ is equal to Nsteps, set

$$\mathbf{T}_{n+1} = \mathbf{T}_{m+1} \quad \text{and} \quad \boldsymbol{\alpha}_{n+1} = \boldsymbol{\alpha}_{m+1} \tag{41}$$

and exit the sub-time stepping loop. Recall that the subscript $(m+1)$ refers to the current *thermal* time step and $(n+1)$ refers to the current *fill* time step.

5. Check fill status of mold and terminate routine if the mold is completely filled. If there are still unfilled nodes, set

$$\mathbf{T}_n = \mathbf{T}_{n+1} \quad \text{and} \quad \boldsymbol{\alpha}_n = \boldsymbol{\alpha}_{n+1} \tag{42}$$

and loop back to Step 1 to compute the next fill time step.

5 Experimental Validations

Since there are currently no experimental results described in literature giving specific details for thick composite sections, results of thin section mold experiments are employed here primarily to validate the present 3-D developments. The additional reason behind the selection of these experiments is that when the mold is sufficiently thin, the 3-D problem readily reduces to a 2-D problem and the results obtained from the 3-D formulations should correspond to those given by the 2-D flow/3-D thermal formulations developed previously by the present authors [Ngo and Tamma (1999, 2000)]. Naturally, in the modeling of thin shell-like geometry, the full 3-D developments are computationally less efficient than the 2-D flow/3-D thermal formulations because the former solve for the flow problem in full three dimensions while the latter assume a two-dimensionally flow field. Comparisons with results obtained from the 2-D flow/3-D thermal formulations are therefore included here for validation purposes only.

5.1 Experiment #1 [Lin, Lee, and Liou (1993)]

The experiment performed by Lin, Lee, and Liou (1993) involves the injection of mixed urethane resin into the circular cavity preplaced with OCF M8610 random fiber mat. The mold cavity has an inner radius of 0.635 cm, an outer radius of 20 cm and a gap thickness of 1.27 cm. According to Lin, Lee, and Liou (1993), the mold walls were kept at a constant temperature of 120°C and the mixed urethane resin was maintained at 41°C prior to injection. Since the filling was carried out using a low pressure sealant gun, the inlet condition was neither a constant pressure nor a constant flow rate. Fig. 2

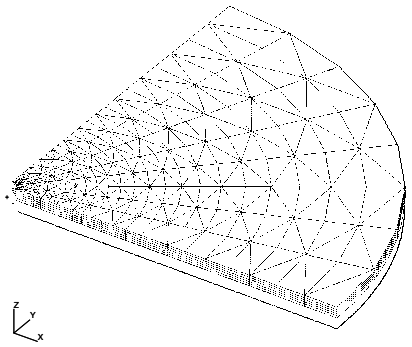

Figure 3 : Finite element mesh used in Experiment #1.

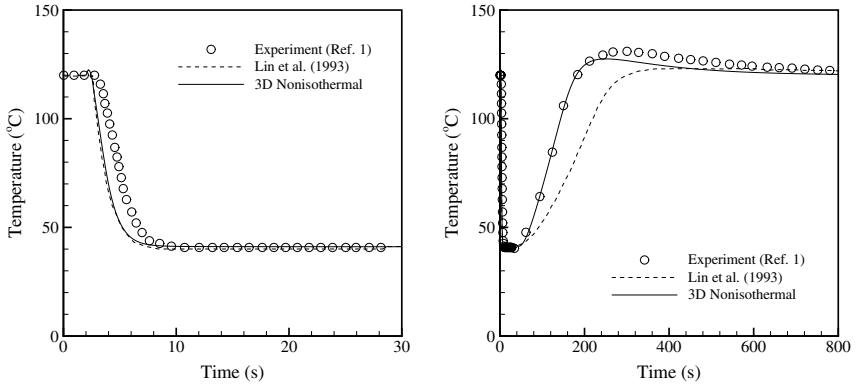

(a) Filling stage (b) Filling and curing stages

Figure 4 : Comparison of predicted temperature to experimental data for Experiment #1 (results plotted as reference location 1).

gives the inlet pressure recorded by Lin et al. during filling and Tab. 1 lists the remaining fiber and resin material properties.

To describe the kinetics behavior of the mixed urethane resin, the following model is used:

$$R_\alpha = A \exp\left(-\frac{E}{RT}\right)(1-\alpha)^n \tag{43}$$

where A, E and n are the kinetics constants whose values are 3.75E+5 s^{-1}, 51941 J/mole and 1.46, respectively, and R is the ideal gas law constant. Lin, Lee, and Liou (1993) describe the viscous behavior of the mixed urethane as

$$\mu = A_\mu \exp\left(\frac{E_\mu}{RT}\right)\left(\frac{\alpha_g}{\alpha_g-\alpha}\right)^{f(\alpha,T)} \tag{44}$$

where A_μ = 1.8E-5 Pa·s, E_μ = 26214 J/mole, and α_g = 0.71. The function $f(\alpha, T)$ in the above Equation (44) is

$$f(\alpha, T) = f(\alpha') = -0.96 + 6.48\alpha' - 3.20(\alpha')^2 \tag{45}$$

where

$$\alpha' = \alpha - \frac{2.13(T - T_{ref})}{374.5 + (T - T_{ref})} \tag{46}$$

and $T_{ref} = 55^oC = 328$ K.

To discretize the circular mold used in the experiment, a finite element consisting of 1296 nodes and 1840 wedge elements is used, Fig. 3. As seen in Fig. 4 through Fig. 6, the results predicted by the present 3-D formulations are in agreement with the trends displayed by the experimental results of Lin, Lee, and Liou (1993). In addition, plots of the current solutions against those obtained by the 2-D flow/3-D thermal formulations [Ngo and Tamma (1999, 2000)] show excellent agreement among the various models, Fig. 7. Therefore, the validity of the 3-D formulations is readily proven.

5.2 Experiment #2 [Chiu, Chen, and Lee (1997)]

In the first of the two sets of non-reactive fluid experiments performed by Chiu, Chen, and Lee (1997), the unidirectional flow measurement device is a rectangular aluminum mold with mold cavity of dimensions 21 cm × 7.63 cm × 0.8 cm. Several thermocouples were used to measure temperature in the cavity during filling and curing, and of importance to the present validation are the temperature results of the thermocouples positioned 0.25L, 0.5L and 0.75L away from the inlet and midway through the cavity thickness. It should be noted that for the non-reactive system, the liquid was pumped and the temperature reading was collected continuously until several minutes after the mold was filled. For the reactive system, the resin flow stopped when the flow front of the resin reached the outlet. However, the temperature data was collected continuously until the temperature returned to the wall temperature after curing [Chiu, Chen, and Lee (1997)].

In the non-reactive non-isothermal mold filling experiment, the fluid used was Palatino oil. The preform used was four layers of a continuous random fiber glass mat (CertainTeed U750), whose properties, along with those of the Palatino oil, are given in Tab. 2. As stated by Chiu, Chen, and Lee (1997), a constant mold wall temperature was obtained by a temperature controller and the fluid was pumped to the mold at a constant flow rate by an Instron machine. Therefore, in the validation of the non-reactive experiment using Palatino oil, the prescribed mold wall temperature is kept at 63°C and the oil temperature is maintained at 34.5°C. The viscosity model of the Palatino oil as described by Chiu, Chen, and Lee (1997) is

$$\mu = 0.001 * \exp\left(\frac{4485.2}{T} - 11.3\right) \tag{47}$$

where μ is in unit of Pa·s.

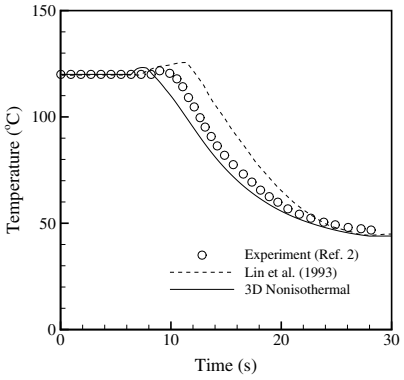

(a) Filling stage

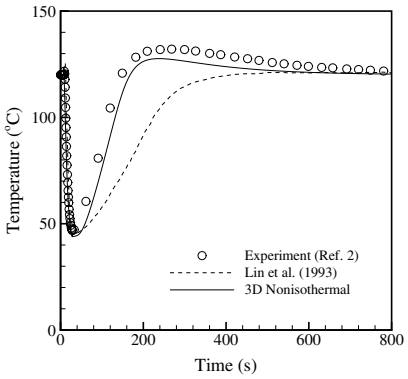

(b) Filling and curing stages

Figure 5 : Comparison of predicted temperature to experimental data for Experiment #1 (results plotted at reference location 2).

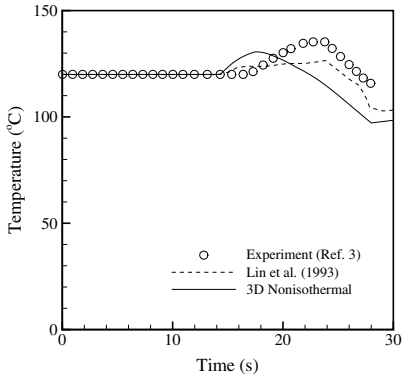

(a) Filling stage

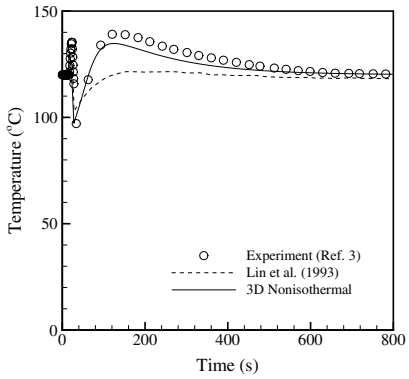

(b) Filling and curing stages

Figure 6 : Comparison of predicted temperature to experimental data for Experiment #1 (results plotted at reference location 3).

To simulate the continuous pumping of the Palatino oil into the mold after the mold was filled (i.e., the Palatino oil was allowed to exit the mold at the other end during filling), a 5 cm run-off area is added to the original length of the discretized mold, bringing to total length to 26 cm. The addition of the run-off area does not affect the temperature results of the validation process in any way because the problem is highly advective and any information downstream of the flow does not play a part in the heat transfer and curing solutions.

Fig. 8 shows the finite element mesh consisting of 1458 nodes and 2080 wedge elements used by the present 3-D methodology. Because of the symmetric nature in the boundary conditions of the experiment (e.g., same prescribed temperature on upper and lower mold walls), only half of the mold along the thickness direction is discretized. As in Fig. 9, the 3-D non-isothermal results follow the general behaviors of the experimental data well. The slight discrepancies between the experimental data and the predicted results can be attributed to experimental errors, lags in thermocouple response, and/or inaccurate viscosity and kinetics parameters inadvertently employed in the present developments. Nevertheless, the virtually indistinguishable nature between the 2-D flow/3-D thermal results and the 3-D non-isothermal results simply confirm the validity of the present developments, Fig. 10.

Table 2 : Material properties: Experiment #2

Parameter	Value
Palatino oil	
Density ρ_f (g/cm^3)	0.98
Heat capacity c_{pf} (J/g·K)	1.88
Thermal conductivity k_f (J/cm·s·K)	0.00136
Fiber	
Density ρ_s (g/cm^3)	2.53
Heat capacity c_{ps} (J/g·K)	0.68
Thermal conductivity k_s (J/cm·s·K)	0.00417
Porosity ϕ	0.91
Permeability $\overline{K}$ (darcy)	4836.1

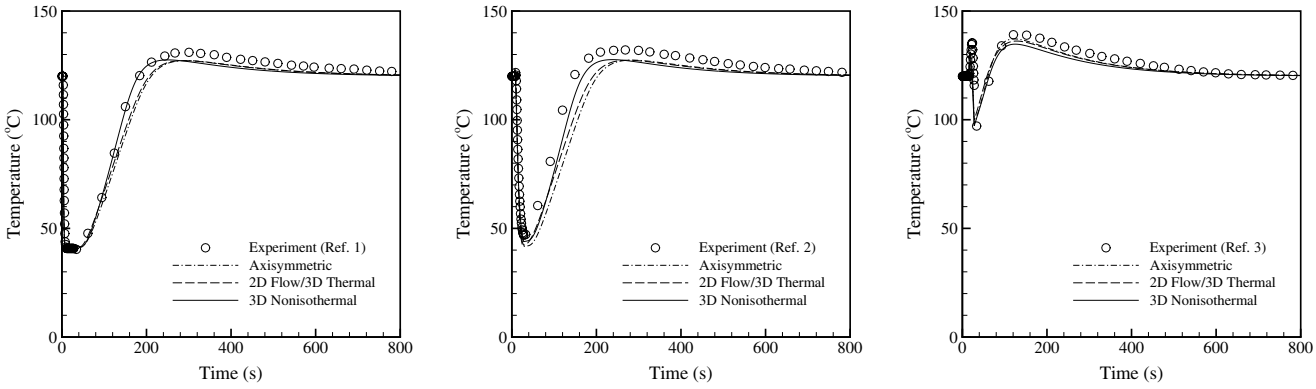

(a) Reference location 1 (b) Reference location 2 (c) Reference location 3

Figure 7 : Comparison of predicted temperatures between various formulations for Experiment #1.

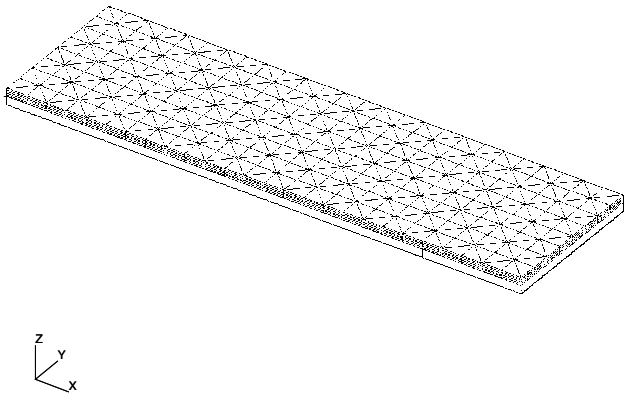

Figure 8 : Finite element mesh used in Experiment #2.

5.3 Experiment #3 [Chiu, Chen, and Lee (1997)]

In the second set of non-reactive fluid experiments performed by Chiu, Chen, and Lee (1997), the experiment utilized the same mold conditions and material properties as in Experiment #2. The main differences between Experiment #3 and Experiment #2 are: (i) that the Palatino oil was injected at a higher flow rate and was maintained at 24°C during filling, and (ii) the mold walls were kept constant at 55°C. The faster flow rate necessitates the inclusion of the phenomenon known as thermal dispersion in the process modeling, and in this study the thermal dispersion conductivity models proposed by Chiu, Chen, and Lee (1997); Wakao and Kaguei (1982) are employed. These are

$$k_D = k_f * 4.2\left[1-\exp\left(-0.2\sqrt{\mathrm{Pe}}\right)\right]\ln(1+\mathrm{Pe}) \tag{48}$$

where Pe is the material Peclet number (not to be confused with the mesh Peclet number) defined by

$$\mathrm{Pe} = \frac{\rho_f c_{pf}}{k_f}|\mathbf{u}|d_f \tag{49}$$

for the model proposed by Chiu, Chen, and Lee (1997), and

$$k_D = k_f * 0.5\mathrm{Pe} \tag{50}$$

for the model developed by Wakao and Kaguei (1982).

Physically, dispersion occurs because the microscopic fluid velocities and temperatures are different form the average values. On the microscopic scale, the fluid moves up and down as it goes around the solid particles, Fig. 11. If the fluid experiences a temperature gradient at the same time it will then convect heat locally, and if these temperature gradients are different from the gradient of the average temperature then there will be a net heat flux [Dessenberger and Tucker (1995)].

Fig. 12 shows that in the absence of thermal dispersion, the predicted temperatures could follow the experiment data in trend only. To get these two set of results to be in excellent agreement with each other, as seen in Fig. 13, the phenomenon of thermal dispersion had to be taken into account via the introduction of an effective thermal dispersion conductivity. Therefore, for manufacturing conditions such as high flow rates, thermal dispersion is a phenomenon that might be considered important. Furthermore, when the modeled geometry is sufficiently thin, the results obtained from a full 3-D non-isothermal methodology readily reduce to those generated by the 2-D flow/3-D thermal methodology [Ngo and Tamma (1999, 2000)], as demonstrated in Fig. 14.

5.4 Experiment #4 [Chiu, Chen, and Lee (1997)]

In the reactive fluid experiment selected as a validation in this study, a fast step growth polymerization is used. According to

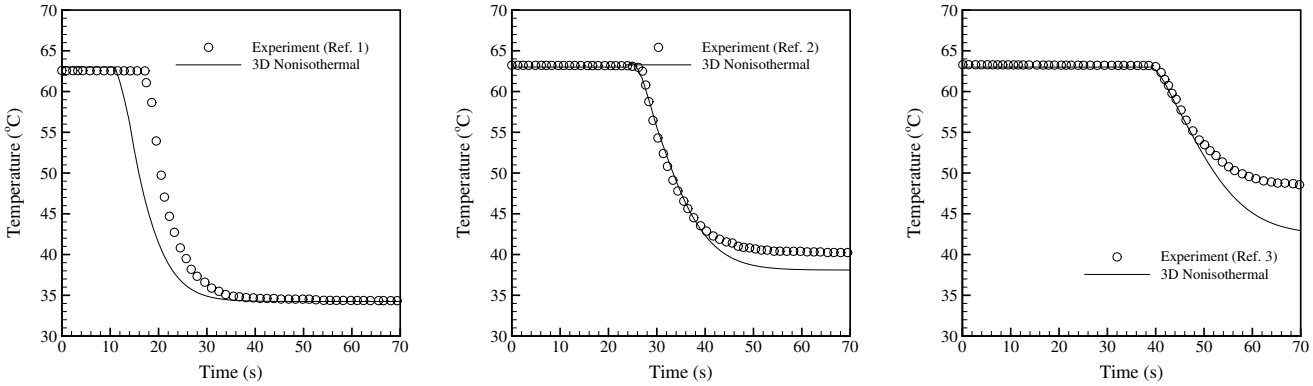

(a) Reference location 1 (b) Reference location 2 (c) Reference location 3

Figure 9 : Comparison of predicted temperature to experimental data for Experiment #2.

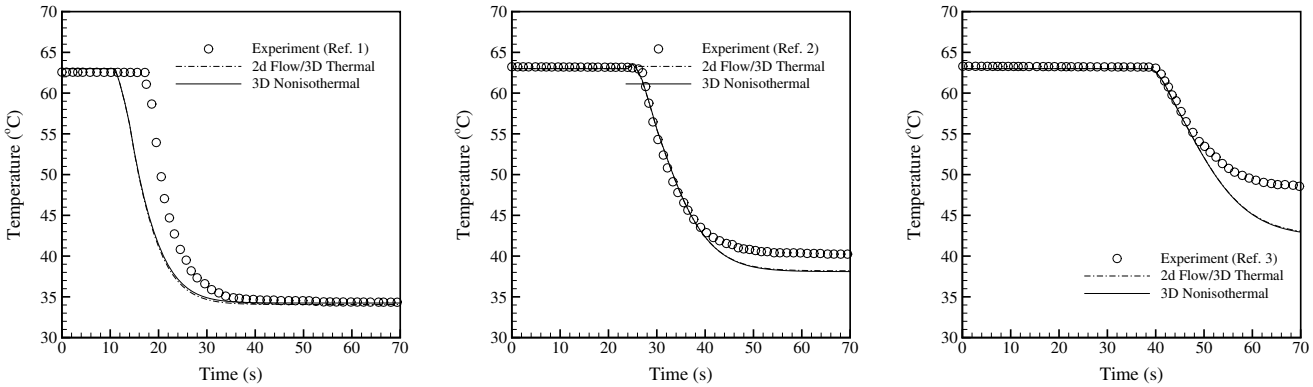

(a) Reference location 1 (b) Reference location 2 (c) Reference location 3

Figure 10 : Comparison of predicted temperatures between various formulations for Experiment #2.

Chiu, Chen, and Lee (1997), the mold was injected with SPECTRIM MM364-A, an isocyanate based on methelyne diphenyl disocyanate and provided by Dow Chemical Company. An adiabatic reactor method was used to determine the cure kinetics of the resin [Chiu, Chen, and Lee (1997); Toth (1995)] and from this method, polyisocyanurate was found to form by a rapid polymerization of isocyanates in the presence of a catalyst. The trimerization or the forming of a polymer from three molecules of a monomer in turn leads to fast gelation and rapid cure. Under the conditions and assumptions listed in Toth (1995), the reaction rate equation can be expressed as:

$$R_\alpha = \frac{K_{A1}\exp\left[-\frac{E_{A1}}{R}\left(\frac{1}{T}-\frac{1}{T_{ref}}\right)\right]C_I^2 C_C}{K_{A42}\exp\left[-\frac{E_{A42}}{R}\left(\frac{1}{T}-\frac{1}{T_{ref}}\right)\right]C_I+1} \tag{51}$$

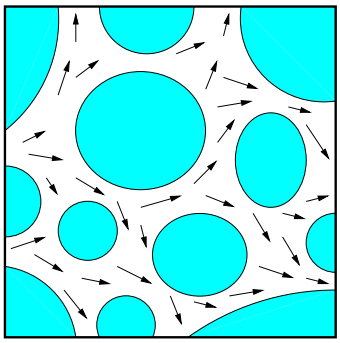

Figure 11 : Local fluid velocity at microscale level.

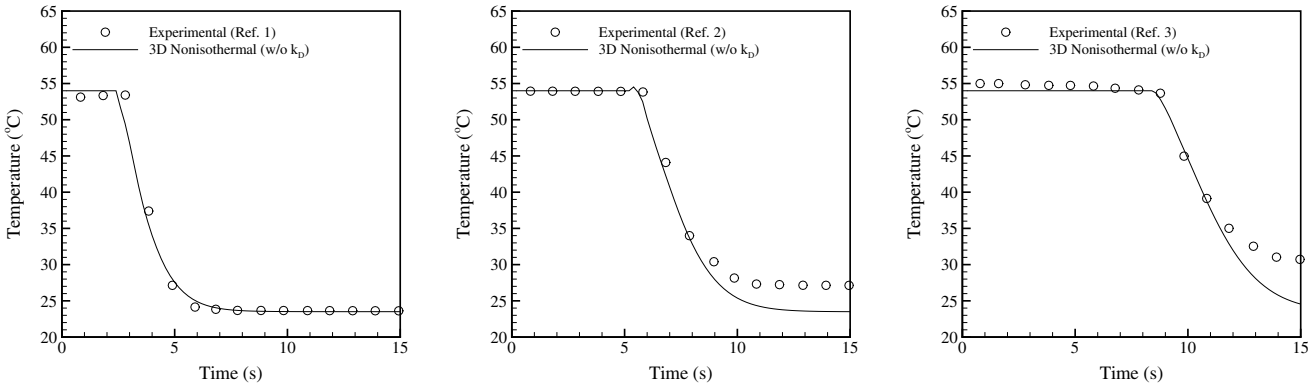

(a) Reference location 1 (b) Reference location 2 (c) Reference location 3

Figure 12 : Comparison of predicted temperature to experimental data for Experiment #3 without k_D.

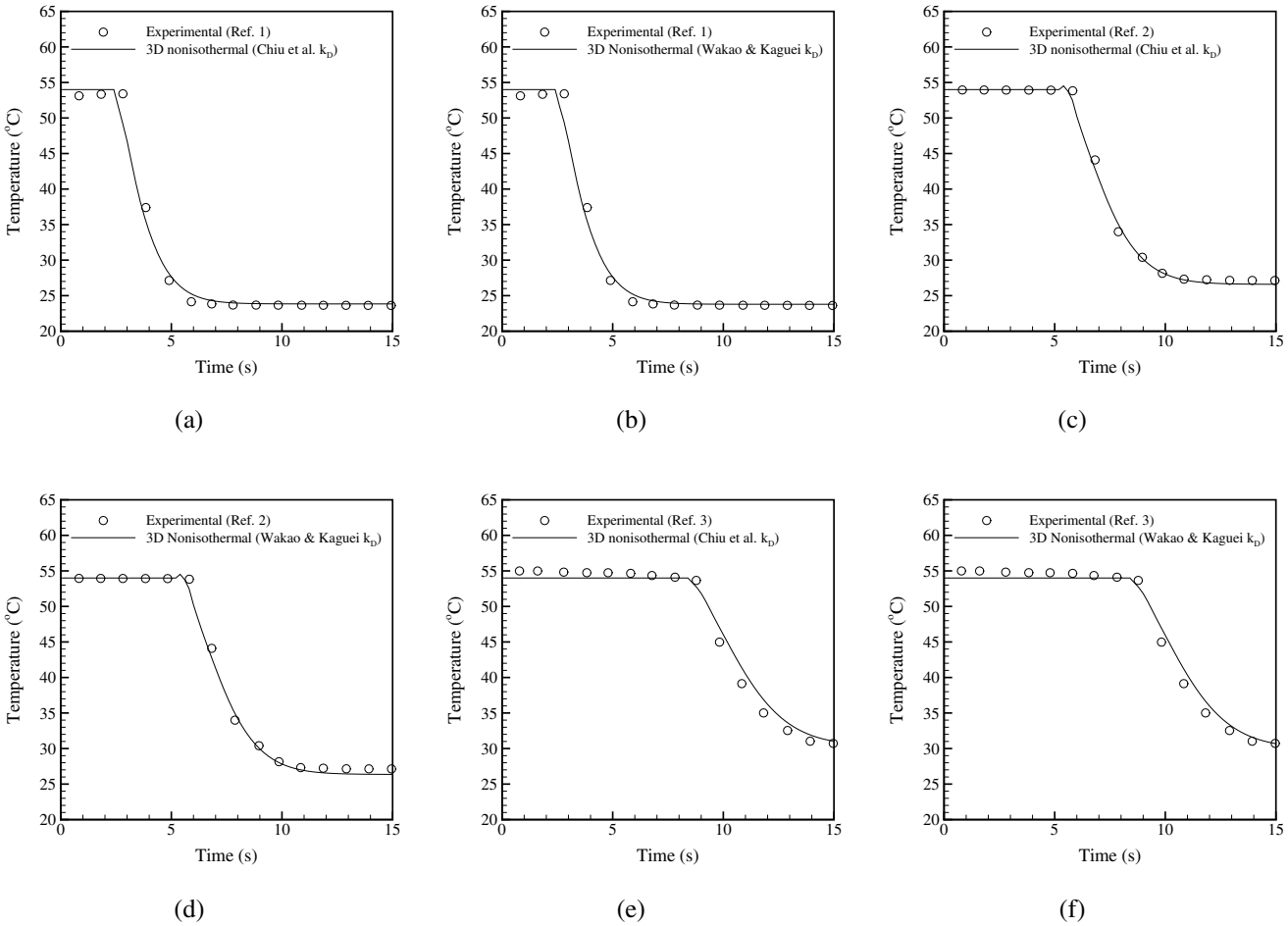

(a) (b) (c)

(d) (e) (f)

Figure 13 : Comparison of predicted temperature to experimental data for Experiment #3 with k_D. (a) Chiu, Chen, and Lee (1997) k_D model (ref 1); (b) Wakao and Kaguei (1982) k_D model (ref 1); (c) Chiu, Chen, and Lee (1997) k_D model (ref 2); (d) Wakao and Kaguei (1982) k_D model (ref 2); (e) Chiu, Chen, and Lee (1997) k_D model (ref 3); (f) Wakao and Kaguei (1982) k_D model (ref 3).

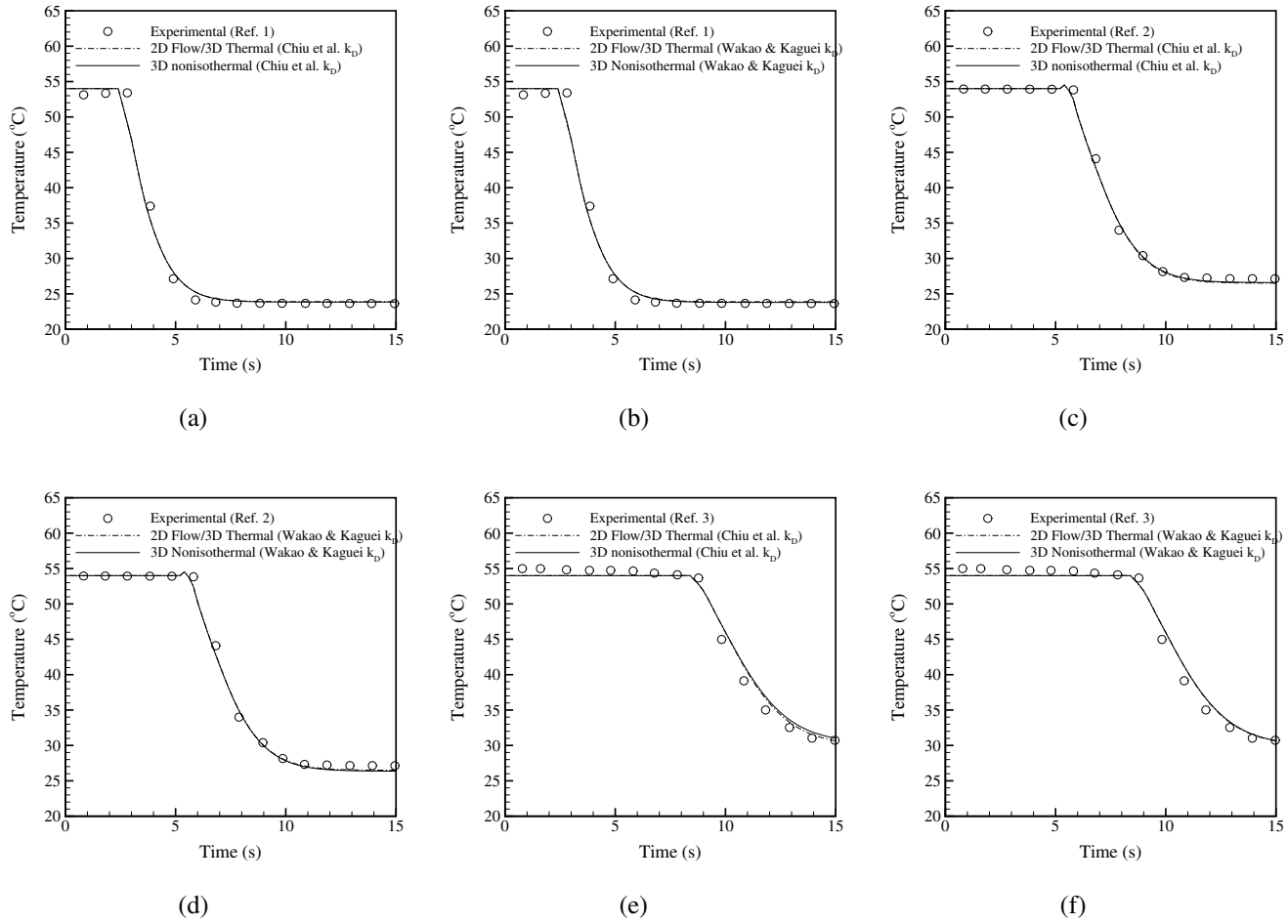

Figure 14 : Comparison of predicted temperatures among various formulations for Experiment #3 with k_D. (a) Chiu, Chen, and Lee (1997) k_D model (ref 1); (b) Wakao and Kaguei (1982) k_D model (ref 1); (c) Chiu, Chen, and Lee (1997) k_D model (ref 2); (d) Wakao and Kaguei (1982) k_D model (ref 2); (e) Chiu, Chen, and Lee (1997) k_D model (ref 3); (f) Wakao and Kaguei (1982) k_D model (ref 3);

where C_I is the isocyanate concentration, C_T is the polyisocyanurate concentration and C_C is the catalyst concentration. Tab. 3 gives the values of C_I and C_C as well as the kinetic parameters K_{A1}, E_{A1}, K_{A42}, E_{A42} and T_{ref} used in the reaction rate equation.

An aluminum mold of dimensions 21 cm $\times$ 7.63 cm $\times$ 0.8 cm is used in the reactive fluid experiment. During injection, the mold walls are kept at 74.3°C and the polyisocyanurate system is maintained at 28.2°C. The material properties of the fiber mat and the polyisocyanurate system are listed in Tab. 4. The mesh used in this validation is shown in Fig. 15 and consists of 1188 nodes and 1680 wedge elements. As in the non-reactive experiments, the use of the same boundary condition on the upper and low mold walls means that only half of the mold cavity needs to be discretized in the simulations.

As seen in Fig. 16, the predicted results obtained from the 3-D non-isothermal formulations are in good agreement with the experiment results. Since the mold is relatively thin by definition, it comes as no surprise that the 3-D non-isothermal results follow the 2-D flow/3-D thermal results extremely well. In fact, these two sets of results are virtually indistinguishable from each other (Fig. 17), further proving that for thin shell-like geometries, the flow in the through thickness direction can be neglected.

6 Concluding Remarks

In the process modeling of thick composite sections, multi-layer preforms with varying characteristics across the different layers, or geometrically complex mold geometries with regions of impermeable inserts via RTM, the assumption of

Table 3 : Model parameters of resin kinetics function: Experiment #4

Parameter	Value
C_I	0.006 023 39
C_C	0.005 623 33
K_{A1} (cm^6/g·mol·s)	$180 + 200\frac{x}{L}$
E_{A1} (J/mol)	8.52E+4
K_{A42} (cm^3/mol)	71.4
E_{A42} (J/mol)	0.0097
T_{ref} (K)	298

Table 4 : Material properties: Experiment #4

Parameter	Value
Polyisocynurate System	
Density ρ_f (g/cm^3)	1.21
Heat capacity c_{pf} (J/g·K)	1.88
Thermal conductivity k_f (J/cm·s·K)	0.002
Heat of reaction H_r (J/g)	1.88E+5
Fiber	
Density ρ_s (g/cm^3)	2.53
Heat capacity c_{ps} (J/g·K)	0.68
Thermal conductivity k_s (J/cm·s·K)	0.00417
Porosity ϕ	0.85
Permeability $\overline{K}$ (darcy)	4836.1

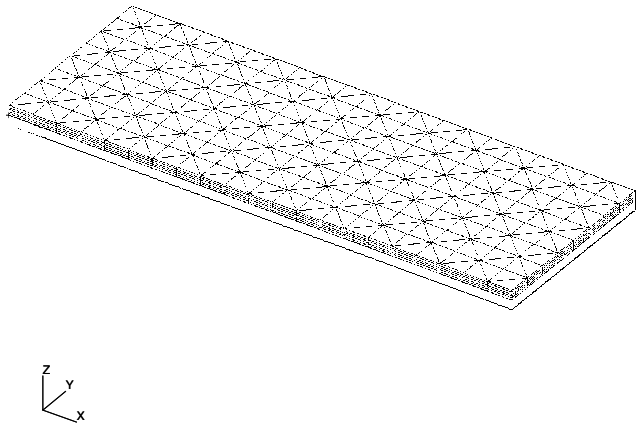

Figure 15 : Finite element mesh used in Experiment #4.

a thin shell-like geometry is no longer valid. The flow in the through thickness direction is no longer negligible and the current practice of treating the flow as two-dimensional and the temperature and cure as three-dimensional are not representative of the underlying physics. In regards to these shortcomings, for the first time, a full three-dimensional integrated methodology is developed in conjunction with an implicit pure Finite Element technique to model and account for the three-dimensional nature of the flow, thermal and curing fields.

All of the results obtained from the present 3-D developments are, in general, in good agreement with the available experimental results. The explicit assumption made in the developments is when the modeled geometry is sufficiently thin, the 3-D problem reduces to a 2-D flow problem with a 3-D temperature and curing fields. Thus, it came as no surprise that in all case studies, the 3-D non-isothermal results are virtually indistinguishable from the 2-D flow/3-D thermal results obtained previously by the authors [Ngo and Tamma (1999, 2000)]. For thick composites geometries, however, such will not be the case and the full 3-D non-isothermal methodology is expected to yield more accurate results. Future examples will be carried out to demonstrate the ability of the present developments to model the various related physical phenomena in thick composite sections, multi-layer preforms with varying characteristics across the different layers, and specifically, geometrically complex mold geometries with regions of embedded impermeable inserts (cited to be of use in structural armor) and the like.

Finally, as it was shown in Experiment #3, under certain situations, the phenomenon of thermal dispersion must be considered when applying porous media theory to fiber-reinforced manufacturing processes. Unfortunately, there are currently no practical methods for determining the thermal dispersion function. Most techniques employed in the determination of the elusive k_D still rely on the process of fitting the numerical results to the experimental data, which can be quite tedious and material dependent.

Acknowledgement: The authors are very pleased to acknowledge support in part by Battelle/U.S. Army Research Office (ARO) Research Triangle Park, North Carolina, under grant number DAAH04-96-C-0086, and by the Army High Performance Computing Research Center (AHPCRC) under the auspices of the Department of the Army, Army Research Laboratory (ARL) cooperative agreement number DAAH04-95-2-0003/contract number DAAH04-95-C-0008. The content does not necessarily reflect the position or the policy of the government, and no official endorsement should be inferred. Support in part by Dr. Andrew Mark of the Integrated Modeling and Testing (IMT) Computational Technical Activity and the ARL/MSRC facilities is also gratefully acknowledged. Special thanks are due to the CICD and the Materials Division of WMRD at the U.S. Army Research Laboratory (ARL), Aberdeen Proving Ground, Maryland. Other related support in form of computer grants from the Minnesota Supercomputer Institute (MSI), Minneapolis, Minnesota is also gratefully acknowledged.

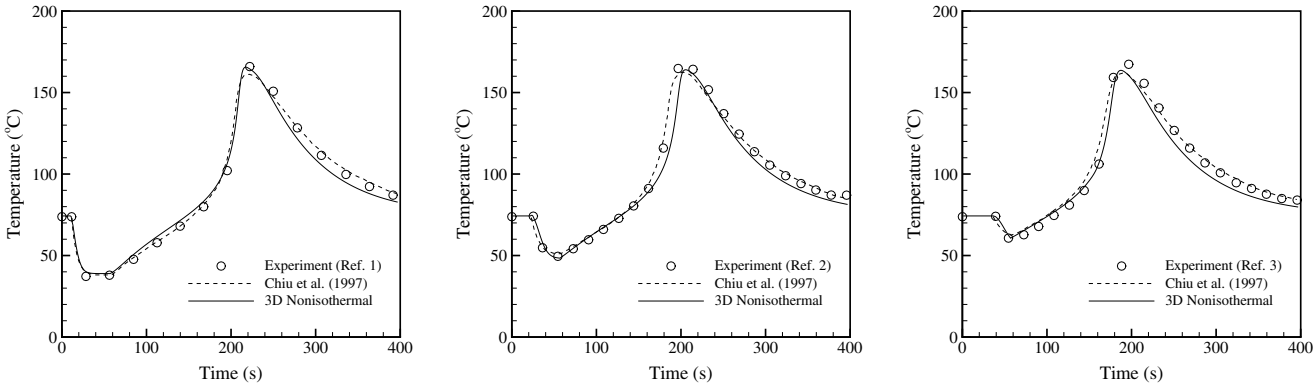

(a) Reference location 1 (b) Reference location 2 (c) Reference location 3

Figure 16 : Comparison of predicted temperature to experimental data for Experiment #4.

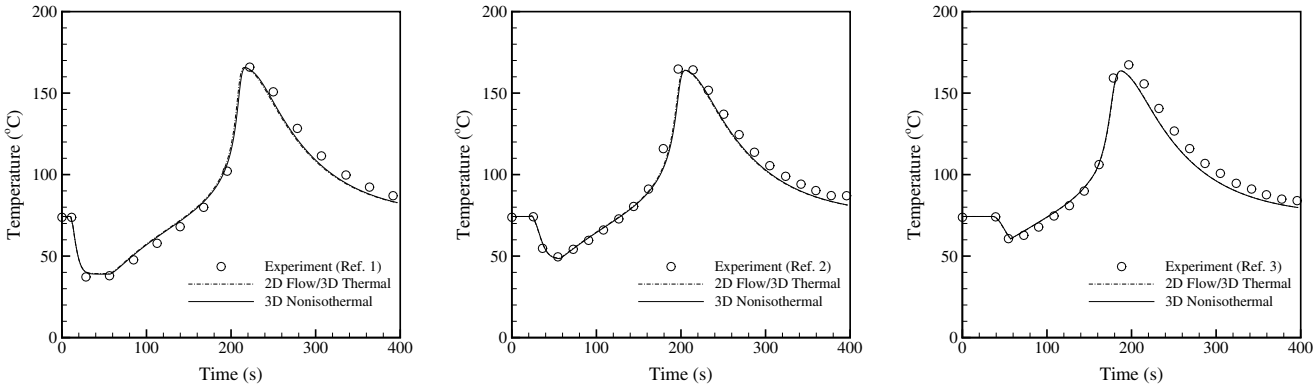

(a) Reference location 1 (b) Reference location 2 (c) Reference location 3

Figure 17 : Comparison of predicted temperatures between various formulations for Experiment #4.

References

Brinkman, H. C. (1947): A Calculation of the Viscous Force Exerted by a Flowing Fluid on a Dense Swarm of Particles. *Applied Scientific Research*, vol. A1, pp. 27–34.

Brooks, A. N.; Hughes, T. J. R. (1982): Streamline Upwind/Petrov-Galerkin Formulations for Convection Dominated Flows with Particular Emphasis on the Incompressible Navier-Stokes Equations. *Computer Methods in Applied Mechanics and Engineering*, vol. 32, pp. 199–259.

Bruschke, M. V.; Advani, S. G. (1994): A Numerical Approach to Model Non-Isothermal Viscous Flow Through Fibrous Media with Free Surfaces. *International Journal for Numerical Methods in Fluids*, vol. 19, pp. 575–603.

Chan, A. W.; Hwang, S. T. (1992): Modeling Resin Transfer Molding of Axisymmetric Composite Parts. *Journal of Materials Processing and Manufacturing Science*, pp. 105–118.

Chan, A. W.; Hwang, S. T. (1993): Modeling Resin Tranfer Molding of Polyimide (PMR-15)/Fiber Composites. *Polymer Composites*, vol. 14, no. 6, pp. 524–528.

Chen, Y. T. (1993): *Resin Transfer Molding of Polycyanate: Chemorheology, Molding Experiments and Wetting Visualization*. PhD thesis, University of Minnesota, 1993.

Chiu, H.; Chen, S. C.; Lee, L. J. (1997): Analysis of Heat Transfer and Resin Reaction in Liquid Composite Molding. *ANTEC '97*, pp. 2424–2429.

Darcy, H. (1856): *Les Fontaines Publiques de la Ville de Dijon*. Delmont, Paris.

Dessenberger, R. B.; Tucker, C. L. (1995): Thermal Dispersion in Resin Transfer Molding. *Polymer Composites*, vol. 16, no. 6, pp. 495–506.

Gao, D. M.; Trochu, F.; Gauvin, R. (1995): Heat Transfer Analysis of Non-Isothermal Resin Transfer Molding by the Finite Element Method. *Materials and Manufacturing Processes*, vol. 10, no. 1, pp. 57–64.

Kaviany, M. (1995): *Principles of Heat Transfer in Porous Media*. Springer, New york, 2nd edition.

Lee, L. J.; Young, W. B.; Lin, R. J. (1994): Mold Filling and Cure Modeling of RTM and SRIM Processes. *Composite Structures*, vol. 27, pp. 109–120.

Lin, R.; Lee, L. J.; Liou, M. J. (1991): Nonisothermal Mold Filling in Resin Transfer Molding and Structural Reaction Injection Molding. In *ANTEC '91*, pp. 815–818.

Lin, R. J.; Lee, L. J.; Liou, M. J. (1993): Mold Filling and Curing Analysis in Liquid Composite Molding. *Polymer Composites*, vol. 14, no. 1, pp. 71–81.

Liu, B.; Advani, S. G. (1995): Operator Splitting Scheme of 3-D Temperature Solution Based on 2-D Flow Approximation. *Computational Mechanics*, vol. 16, pp. 74–82.

Mohan, R. V.; Ngo, N. D.; Tamma, K. K. (1999): On a Pure Finite Element Methodology for Resin Transfer Mold Filling Simulations. *Polymer Engineering and Science*, vol. 39, no. 1.

Mohan, R. V.; Ngo, N. D.; Tamma, K. K. (1999): Three-Dimensional Resin Transfer Molding: Part 1–Isothermal Process Modeling and Explicit Tracking of Moving Fronts for Thick Geometrically Complex Composites Manufacturing Applications. *Numerical Heat Transfer, Part A–Applications*, vol. 35, pp. 815–838.

Mohan, R. V.; Ngo, N. D.; Tamma, K. K.; Shires, D. R. (1999): Three-Dimensional Resin Transfer Molding: Part 2–Isothermal Process Modeling and Implicit Tracking of Moving Fronts for Thick Geometrically Complex Composites Manufacturing Applications. *Numerical Heat Transfer Part A–Applications*, vol. 35, no. 8, pp. 839–858.

Mohan, R. V.; Shires, D. R.; Tamma, K. K.; Ngo, N. D. (1998): Flow Channels and Fiber Impregnation Studies for the Process Modeling/Analysis of Complex Engineering Structures Manufactured by Resin Transfer Molding. *Polymer Composites*, vol. 19, no. 5, pp. 527–542.

Ngo, N. D.; Mohan, R. V.; Chung, P. W.; Tamma, K. K. (1997): Recent Developments Encompassing Non-Isothermal/Isothermal Liquid Composite Molding Process Modeling/Analysis: Computationally Effective and Affordable Simulations and Validations. *Journal of Thermoplastic Composite Materials*. Submitted to special issue on Affordable Composite Materials and Processing, Journal of Thermoplastic Composite Materials, ASME International Congress and Exhibition, Dallas, TX.

Ngo, N. D.; Tamma, K. K. (1999): Non-Isothermal "2-D Flow/3-D Thermal" Developments Encompassing Process Modeling of Composites: Flow/Thermal/Cure Formulations and Validations Proceedings. In *1999 International Mechanical Engineering Congress and Exposition, IMECE '99*.

Ngo, N. D.; Tamma, K. K. (2000): Non-Isothermal "2-D Flow/3-D Thermal" Developments Encompassing Process Modeling of Composites: Flow/Thermal/Cure Formulations and Validations. *International Journal for Numerical Methods in Engineering*. Submitted for printing.

Toth, J. (1995): Material Characterization in Liquid Injection/Compression Molding. Master's thesis, Ohio State University, 1995.

Trochu, F.; Boudreault, J. F.; Gao, D. M.; Gauvin, R. (1995): Three-Dimensional Flow Simulations for the Resin Transfer Molding Process. *Materials and Manufacturing Processes*, vol. 10, no. 1, pp. 21–26.

Trochu, F.; Gauvin, R.; Gao, D. M. (1993): Numerical Analysis of the Resin Transfer Molding Process by the Finite Element Method. *Advances in Polymer Technology*, vol. 12, no. 4, pp. 329–342.

Trochu, F.; Gauvin, R.; Zhang, Z. (1992): Simulation of Mold Filling in Resin Transfer Molding by Non-Conforming Finite Elements. In *International Conference on Computer Aided Design in Composite Material Technology*, pp. 109–120.

Tucker, C. L.; Dessenberger, R. B. (1994): *Flow and Rheology in Polymer Composites Manufacturing*, chapter 8. Elsevier Science, 1994.

Wakao, N.; Kaguei, S. (1982): *Heat and Mass Transfer in Packed Beds*. Gordon and Breach, New York.

Young, W. B. (1994): Three-Dimensional Nonisothermal Mold Filling Simulations in Resin Transfer Molding. *Polymer Composites*, vol. 15, no. 2, pp. 118–127.

Young, W. B. (1995): Thermal Behaviors of the Resin and Mold in the Process of Resin Transfer Molding. *Journal of Reinforced Plastics and Composites*, vol. 14, pp. 310–332.